Finite-Element Analysis of Complex Axisymmetric Radiating Structures

Andrew D. Greenwood, *Member, IEEE* and Jian-Ming Jin, *Senior Member, IEEE*

***Abstract*— A finite-element method (FEM) is developed for the analysis of complex axisymmetric radiating structures. The method is based on the electric field formulation with the transverse field expanded in terms of edge-based vector basis functions and the azimuth component expanded using nodal-based scalar basis functions. This mixed representation of the electric field eliminates spurious solutions and permits an easy treatment of boundary conditions on conducting surfaces as well as across material interfaces. The FEM mesh is truncated using a recently developed cylindrical perfectly matched layer (PML). The method has been successfully applied to three radiating structures: a corrugated horn antenna, a spherical Luneburg lens, and a half Maxwell fish eye. Numerical results are presented to show the validity, accuracy, and efficiency of the method.**

***Index Terms*— Antennas, bodies of revolution, finite-element methods.**

I. Introduction

AXISYMMETRIC radiating structures with a nonaxisymmetric source are an important class of antennas. Often, these radiating structures are electrically large, necessitating efficient and accurate computational techniques. A common method is the method of moments (MoM) using integral equation formulations [1]–[5]. However, these techniques have limited material handling capabilities since they are not efficient when inhomogeneous materials are present. The finite-element method (FEM) is characterized by very flexible material handling capabilities and is often preferred over the MoM for problems involving complex structures and inhomogeneous materials [6]–[9]. The main issues with the FEM arise from two sources. First, it is necessary to truncate the FEM mesh with an appropriate absorbing boundary condition (ABC), and second, the FEM formulation must be free of spurious solutions.

A variety of approaches to the axisymmetric antenna analysis are found in the literature. All of the approaches reduce the three-dimensional (3-D) problem to a two-dimensional (2-D) computational domain by taking advantage of the rotational symmetry. Mei pioneered the finite-element analysis of axisymmetric antennas using the so-called unimoment method [6]. This method is based on the coupled azimuth potential (CAP) formulation [10], which describes the problem in terms of E_ϕ and H_ϕ. Both field components are everywhere continuous due to the rotational symmetry and the formulation is free of spurious modes. However, when the other field components are computed from E_ϕ and H_ϕ, the CAP formulation can suffer from an imperfect cancellation problem, which limits the accuracy of the results [11], [12]. The FEM mesh in the unimoment method is truncated with a spherical harmonic expansion. While exact, it requires a spherical mesh boundary, which is computationally inefficient for elongated geometries. The FEM with the CAP formulation is also employed to investigate the effect of a radome on the radiation of an antenna [7]. However, the FEM mesh here is truncated using an approximate boundary condition derived from the Wilcox expansion theorem. In addition to the inaccuracy of the approximate boundary condition, the method also suffers from the inherited drawback of the CAP formulation. This drawback can by avoided by formulating the antenna problem in terms of the electric field, which is expanded using edge-based vector basis functions for the field component transverse to ϕ and nodal-based scalar basis functions for the ϕ component [8], [9], [13]–[16]. This mixed representation automatically satisfies the boundary conditions at material discontinuities and sharp conductor edges. In addition, the use of edge-based vector basis functions to expand the transverse field eliminates spurious modes. In [8], the FEM is hybridized with the MoM to create an exact ABC. This hybrid method results in a matrix equation, which is partially sparse and partially full and, thus, computationally difficult to handle. In [9], the FEM mesh is truncated with a spherical harmonic expansion, as done in the unimoment method. As indicated earlier, this truncation is computationally inefficient for elongated geometries.

The use of a perfectly matched layer (PML) for mesh truncation presents convenient computational advantages. For example, PML is available in cylindrical coordinates [17]–[19], resulting in a computationally efficient domain for almost any geometry. Further, PML can be used without altering the sparsity of the FEM matrix, and although PML is an approximate mesh truncation, it can be made very accurate, allowing it to be placed near the radiating geometry. Finally, when using PML, reflection errors can be systematically controlled. For a more accurate mesh truncation, one needs only to increase the thickness of the PML region.

Because of the potential computational advantages, this paper investigates the use of a mixed edge-nodal FEM basis scheme with a PML mesh truncation for the solution of antenna radiation problems. Section II discusses the formulation

Manuscript received July 27, 1998; revised April 9, 1999. This work was supported by a Grant from AFOSR via the MURI Program under contract F49620–96–1–0025.

A. D. Greenwood is with the Air Force Research Laboratory, Directed Energy Directorate, Kirtland AFB, NM 87117 USA.

J.-M. Jin is with the Electrical and Computer Engineering Department, University of Illinois, Urbana, IL 61801 USA.

Publisher Item Identifier S 0018-926X(99)07952-1.

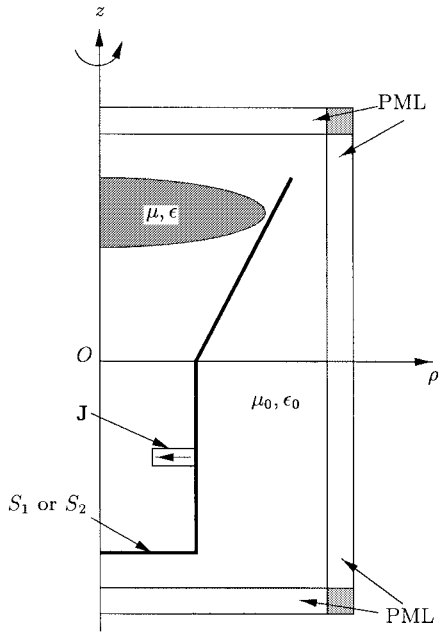

Fig. 1. Diagram of a typical computational domain.

of the method. In Section III, modeling of source currents is discussed. Section IV gives some numerical results and concluding remarks are given in Section V.

II. Formulation

An example of a typical computational domain is shown in Fig. 1. The domain is truncated with cylindrical PML, which is conveniently interpreted as an anisotropic medium [19]. Thus, the permittivity and permeability in the domain are given by

$$\begin{aligned} \epsilon &= \epsilon_0 \epsilon_r \bar{\bar{\Lambda}} \\ \mu &= \mu_0 \mu_r \bar{\bar{\Lambda}} \end{aligned} \tag{1}$$

in which $\bar{\bar{\Lambda}}$ is a diagonal tensor given by

$$\bar{\bar{\Lambda}} = \hat{\rho}\hat{\rho}\Lambda_\rho + \hat{\phi}\hat{\phi}\Lambda_\phi + \hat{z}\hat{z}\Lambda_z. \tag{2}$$

The properties of the PML are contained in $\bar{\bar{\Lambda}}$ and a discussion of appropriate functions for Λ_ρ, Λ_ϕ, and Λ_z is found in [13].

The formulation begins with the vector wave equation

$$\nabla \times \frac{1}{\mu_r} \bar{\bar{\Lambda}}^{-1} \cdot \nabla \times \mathbf{E} - k_0^2 \epsilon_r \bar{\bar{\Lambda}} \cdot \mathbf{E} = -jk_0\eta_0 \mathbf{J} \tag{3}$$

where $k_0 = \omega\sqrt{\mu_0\epsilon_0}$ is the free-space wavenumber, $\eta_0 = \sqrt{\mu_0/\epsilon_0}$ is the impedance of free-space, and $\mathbf{J}$ is a source current density. The boundary conditions are

$$\hat{n} \times \mathbf{E} = 0 \quad \text{on } S_1 \tag{4}$$

where S_1 is the surface of a perfect electric conductor (PEC) and

$$\frac{1}{\mu_r} \hat{n} \times \bar{\bar{\Lambda}}^{-1} \cdot (\nabla \times \mathbf{E}) + \gamma_e \hat{n} \times \hat{n} \times \mathbf{E} = 0 \quad \text{on } S_2 \tag{5}$$

where S_2 is the surface of an impenetrable material with an impedance boundary condition. Any convenient boundary condition can be applied at the outer edge of the domain, which is lined with PML. Usually, (4) is used because this choice reduces the number of unknowns in the FEM system.

The wave equation in (3) is self adjoint and from the generalized variational principle [20], the corresponding functional is

$$\begin{aligned} F(\mathbf{E}) = \frac{1}{2} \iiint_V \Big[&\frac{1}{\mu_r} (\nabla \times \mathbf{E}) \cdot \bar{\bar{\Lambda}}^{-1} \cdot (\nabla \times \mathbf{E}) \\ &- k_0^2 \epsilon_r \mathbf{E} \cdot \bar{\bar{\Lambda}} \cdot \mathbf{E} \Big] \, dV \\ &+ \frac{1}{2} \iint_{S_2} \gamma_e [\mathbf{E} \cdot \mathbf{E} - (\hat{n} \cdot \mathbf{E})(\hat{n} \cdot \mathbf{E})] \, dS \\ &+ jk_0\eta_0 \iiint_V \mathbf{E} \cdot \mathbf{J} \, dV. \end{aligned} \tag{6}$$

To take advantage of the rotational symmetry of the problem, $\mathbf{E}$ and $\mathbf{J}$ are expanded into Fourier components as

$$\mathbf{E} = \sum_{m=-\infty}^{\infty} [\mathbf{E}_{t,m}(\rho, z) + \hat{\phi} E_{\phi,m}(\rho, z)] e^{jm\phi} \tag{7}$$

$$\mathbf{J} = \sum_{m=-\infty}^{\infty} [\mathbf{J}_{t,m}(\rho, z) + \hat{\phi} J_{\phi,m}(\rho, z)] e^{jm\phi} \tag{8}$$

and these are substituted into (6). This allows the ϕ integrations to be explicitly performed and reduces the 3-D problem to a 2-D computational domain.

To avoid nonintegrable singularities in the functional, the FEM expansions must satisfy the appropriate field conditions at $\rho = 0$. The FEM expansions that satisfy this criteria are [13], [21]

$$\begin{aligned} E_{\phi,0} &= \sum_{i=1}^{N_n} e_{\phi,i} N_i \\ \mathbf{E}_{t,0} &= \sum_{i=1}^{N_s} e_{t,i} \mathbf{N}_i \end{aligned} \tag{9}$$

for $m = 0$,

$$\begin{aligned} E_{\phi,\pm 1} &= \sum_{i=1}^{N_n} e_{\phi,i} N_i \\ \mathbf{E}_{t,\pm 1} &= \mp j\hat{\rho} \sum_{i=1}^{N_n} e_{\phi,i} N_i + \sum_{i=1}^{N_s} e_{t,i} \rho \mathbf{N}_i \end{aligned} \tag{10}$$

for $m = \pm 1$, and

$$\begin{aligned} E_{\phi,m} &= \sum_{i=1}^{N_n} e_{\phi,i} N_i \\ \mathbf{E}_{t,m} &= \sum_{i=1}^{N_s} e_{t,i} \rho \mathbf{N}_i \end{aligned} \tag{11}$$

for $|m| > 1$. In the above expansions, N_n and N_s represent the number of nodes and the number of segments (or edges), respectively, in the FEM mesh, $e_{\phi,i}$ and $e_{t,i}$ are the unknown expansion coefficients, and N_i and $\mathbf{N}_i$ represent the standard

linear (first-order) nodal and edge-element basis functions. Within a given triangular element of the FEM mesh, there are three nodal and three edge-element basis functions. The three nodal basis functions are given by $N_i^e = \lambda_i^e$ where λ_i^e denote the area coordinates for element e [20]. Further, if the edge from node 1 to node 2 is numbered 1, the edge from node 2 to node 3 is numbered 2, and the edge from node 3 to node 1 is numbered 3, the edge element basis functions are given by

$$\mathbf{N}_i^e = \ell_i^e \left(\lambda_i^e \nabla_t \lambda_l^e - \lambda_l^e \nabla_t \lambda_i^e\right) \tag{12}$$

where i denotes the edge number, l denotes one plus the remainder of the integer division $i/3$, ℓ_i^e denotes the length of edge i, and $\nabla_t = \hat{\rho}\frac{\partial}{\partial \rho} + \hat{z}\frac{\partial}{\partial z}$.

The expansions in (9)–(11) are substituted into (6) and the functional is extremized by differentiating with respect to the unknown coefficients and then setting the result to zero. This process yields a sparse, symmetric matrix equation, which is solved according the techniques described in [13]. The far-field radiation pattern of the system is computed by integrating the near-field result over a contour in the FEM domain similar to the computation of the radar cross section in [13].

III. Modeling of Source Currents

The geometry of a radiation problem may be rotationally symmetric, but the source current often exists at a specific location in ϕ. If a source current at a specific ϕ location has a finite thickness in ϕ, it can be modeled as a Fourier series for the rotationally symmetric FEM solution. Consider the volume source current density given by

$$\mathbf{J} = \begin{cases} \mathbf{A}(\rho, z), & \phi_0 - \Delta/2 \le \phi \le \phi_0 + \Delta/2 \\ 0, & \text{else} \end{cases} \tag{13}$$

where $\mathbf{A}$ is a complex vector specifying the magnitude, direction, and phase of the current. This current can be written in Fourier series form as

$$\mathbf{J} = \frac{\mathbf{A}\Delta}{2\pi} \sum_{m=-\infty}^{\infty} \frac{\sin(m\Delta/2)}{m\Delta/2} e^{jm(\phi-\phi_0)}. \tag{14}$$

The Fourier series is truncated after a finite number of terms. The number of terms (or modes) that must be computed depends on the maximum error tolerable in the Fourier series approximation to the current. The current can be further decomposed as

$$\begin{aligned} \mathbf{J}_{t,m} &= \mathbf{J}_{t,m}^e + \mathbf{J}_{t,m}^o \\ J_{\phi,m} &= J_{\phi,m}^e + J_{\phi,m}^o \end{aligned} \tag{15}$$

where $\mathbf{J}_{t,m}^e$ and $J_{\phi,m}^e$ are even functions of m and $\mathbf{J}_{t,m}^o$ and $J_{\phi,m}^o$ are odd functions of m. This allows the FEM solution for negative numbered modes to be deduced by symmetry properties. The elimination of the negative numbered modes is a significant computational savings.

In addition to modeling source currents, it is also useful to consider fields incident in waveguides as excitations to radiating systems. This eliminates the need to model long waveguide feeds, which is computationally expensive. Consider the infinitely long waveguide feed shown in Fig. 2(a)

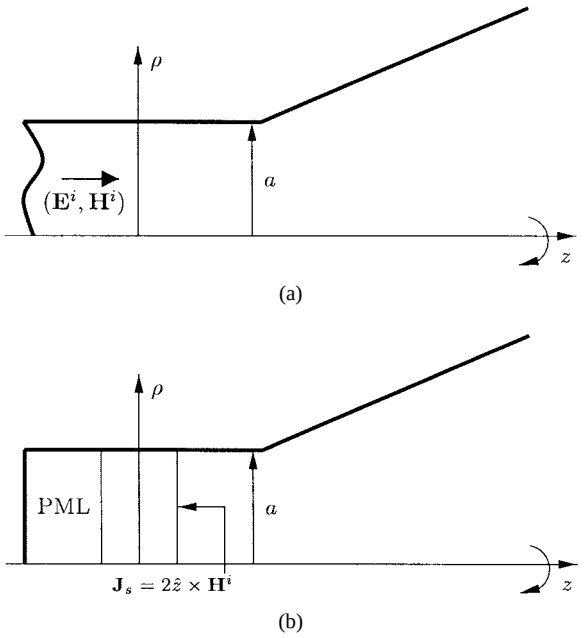

Fig. 2. Model of a waveguide excitation. (a) Original problem. (b) Finite model.

TABLE I
Memory and CPU Requirements for a 122 MFlop DEC Alpha Workstation

Problem	Number of Unknowns	Matrix Half-Bandwidth	Number of modes	Memory (Mbytes)	CPU Time (min.)
Corrugated Horn	78,235	435	61	83	64.0
4λ Luneburg Lens	22,086	314	8	25	1.8
7λ Luneburg Lens	56,954	550	8	93	14.2
10λ Luneburg Lens	108,090	771	8	234	58.0
4λ Half Fish-Eye	13,194	345	8	16	1.2
7λ Half Fish-Eye	31,774	537	8	50	7.2
10λ Half Fish-Eye	58,662	730	8	118	26.6

where a known mode distribution is incident from the $-\hat{z}$ direction. This is modeled as shown in Fig. 2(b) where the surface current $\mathbf{J}_s = 2\hat{z} \times \mathbf{H}^i$ is computed from the known incident mode distribution. The surface current launches both a positive traveling wave, which is equivalent to the original incident wave and a negative traveling wave, which is attenuated in the PML. The PML also attenuates any waves which travel in the $-\hat{z}$ direction after being reflected by discontinuities in the waveguide. Thus, when looking in the $-\hat{z}$ direction, the waveguide appears infinitely long although the computational model is short and efficient. Similar to the volume source current model, the surface current $\mathbf{J}_s$ can be written in terms of an even function of m and an odd function of m, eliminating the need to compute negative numbered modes in the FEM system.

IV. Numerical Results

To show the validity and capability of the method, radiation patterns from three different radiating systems are presented, and information about the resources to compute the results is given in Table I. The first radiating system is a corrugated horn antenna. Corrugated horn antennas are extensively investigated in [22] as antennas which can radiate a circularly polarized

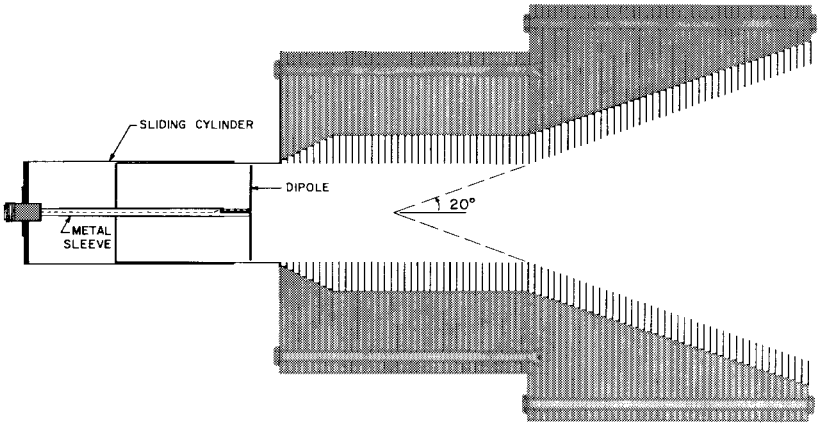

Fig. 3. Diagram of the corrugated horn antenna (reproduced from [22]).

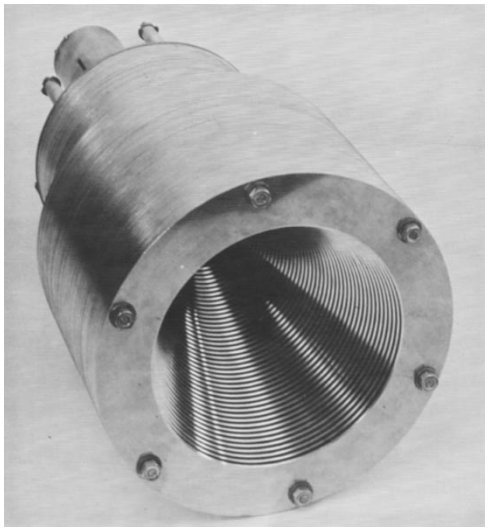

Fig. 4. Photo of the corrugated horn antenna (reproduced from [22]).

wave over a wide beamwidth and a wide bandwidth. As part of the investigation, measurements on several corrugated horn antennas are presented. A diagram showing one such antenna is shown in Fig. 3. The antenna is constructed by bolting together metal washers with thicknesses alternating between 0.079 38 cm and 0.3175 cm. In the section of the waveguide in front of the 20° flare, the washers have inner radii of 3 cm and 4.8 cm, respectively. A photograph of the antenna is shown in Fig. 4. Measurements of the radiation pattern of this antenna at several frequencies are given in [22]. The radiation pattern is computed by the FEM at three frequencies and the FEM and measured results are shown in Figs. 5–7. The agreement between the FEM results and the measured results is excellent. At power levels above -30 dB, note the agreement between the FEM and measurement in predicting slight offsets in the E- and H-plane patterns with respect to each other.

The next radiating system is a spherical Luneburg lens [23] excited by a Hertzian dipole at its surface. The Luneburg lens has a permittivity given by

$$\epsilon_r(r) = 2 - \left(\frac{r}{a}\right)^2 \quad (0 \le r \le a) \tag{16}$$

where a denotes the radius of the lens and r denotes the distance from the center of the lens. The flexibility of the FEM in modeling inhomogeneous materials makes it ideal for the analysis of this system. The Luneburg lens is commonly described by a geometrical optics ray picture, which indicates that spherical waves emitted by a point source placed in the rim of the lens are converted to local plane waves by the lens making the radiation of the system highly directive. The transmitting beam can be steered by moving the antenna feed. The transmitting beam radiation patterns computed by the FEM for Luneburg lenses of 4λ, 7λ, and 10λ diameters (λ is the free-space electromagnetic wavelength) excited by a Hertzian dipole are shown in Fig. 8. As expected, the radiation is directive, and it becomes more directive as the size of the lens increases. In Fig. 8, note that the E- and H-plane patterns are symmetric, so one half of each pattern is shown on the same polar plot. The sidelobe level is at -15 dB. Similar radiation patterns for Luneburg lenses are given in [24], but these patterns are not identical to those given here because a different source on the surface of the lens is used. The field distribution in the 10λ-diameter lens is displayed in Fig. 9, where the absolute value of the real part of the electric field is shown. The figure shows how a spherical wave emitted by the dipole is converted into a wave with a locally planar phase front.

The final radiating system presented is a Hertzian dipole on the surface of a half Maxwell fish eye [25]. The permittivity of the Maxwell fish eye is given by

$$\epsilon_r(r) = \frac{4}{[1 + (r/a)^2]^2} \quad (0 \le r \le a) \tag{17}$$

and a geometrical optics ray picture shows that the spherical waves from a point source are converted to a local plane wave at the center of the lens and then focused to a point on the other side of the lens. Thus, if only one half of the lens is present, the radiation is directive. Radiation patterns computed by the FEM for half Maxwell fish eyes of 4λ, 7λ, and 10λ diameters excited by a Hertzian dipole are shown in Fig. 10. The sidelobe level is at -20 dB, which is about 5 dB lower than in the case of the Luneburg lens. However, compared to the Luneburg lens, the half Maxwell fish eye has two disadvantages. First, it

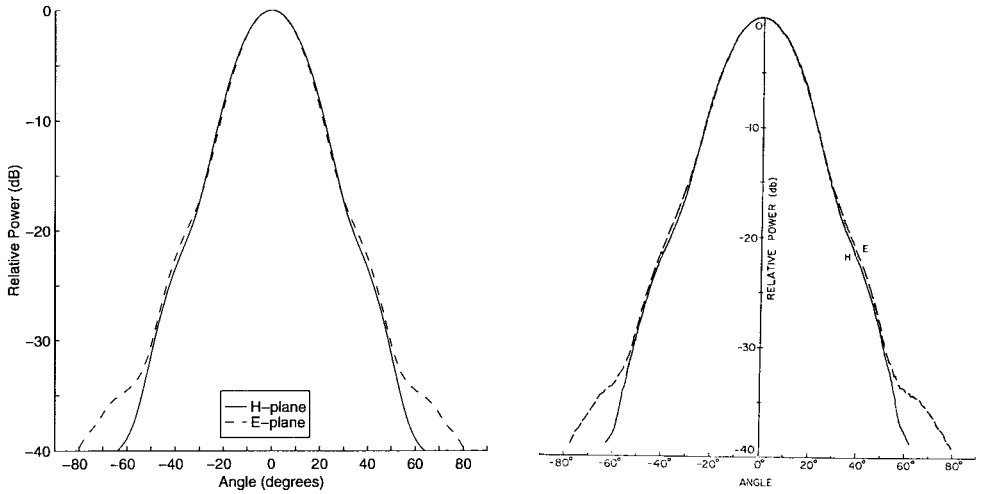

(a) (b)

Fig. 5. Radiation pattern of the corrugated horn antenna at 5.2 GHz (measured results reproduced from [22]). (a) FEM. (b) Measured.

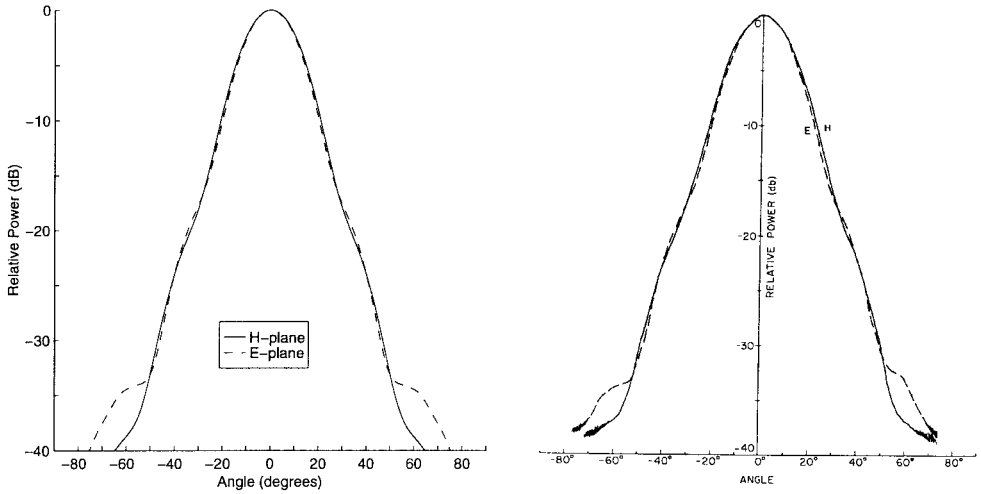

(a) (b)

Fig. 6. Radiation pattern of the corrugated horn antenna at 5.5 GHz (measured results reproduced from [22]). (a) FEM. (b) Measured.

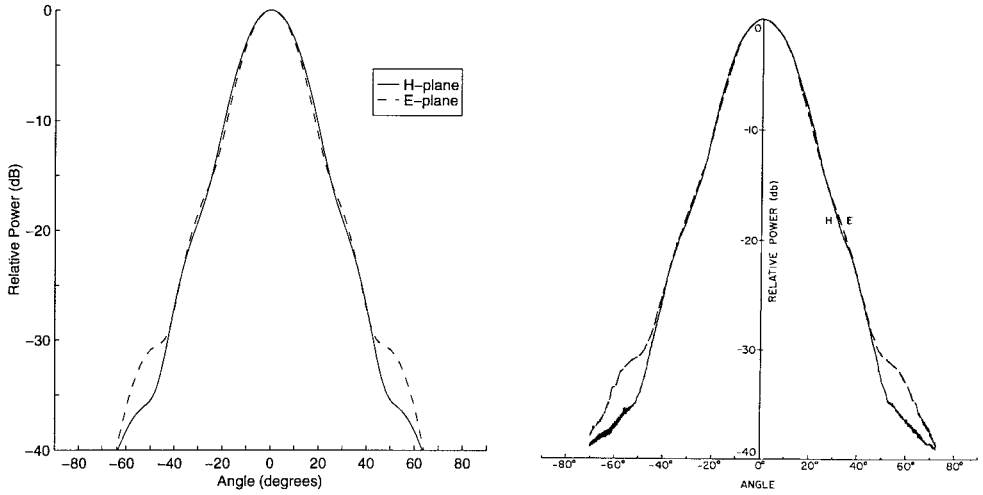

(a) (b)

Fig. 7. Radiation pattern of the corrugated horn antenna at 6.0 GHz (measured results reproduced from [22]). (a) FEM. (b) Measured.

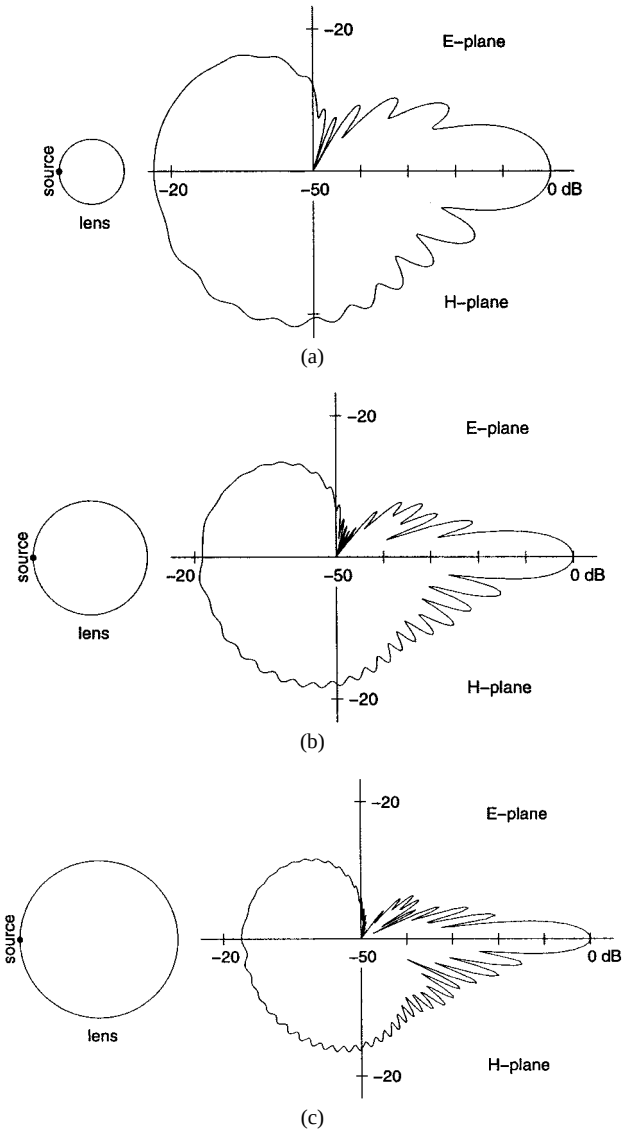

Fig. 8. Radiation from a spherical Luneburg lens excited by a Hertzian dipole. (a) 4λ diameter. (b) 7λ diameter. (c) 10λ diameter.

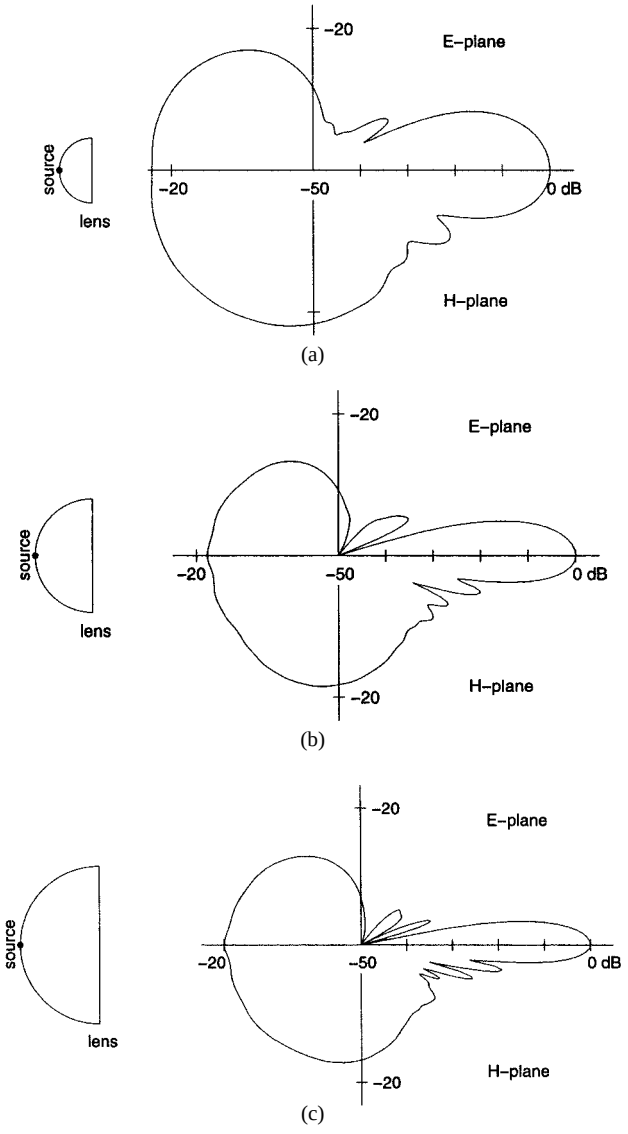

Fig. 10. Radiation from a half Maxwell fish eye excited by a Hertzian dipole. (a) 4λ diameter. (b) 7λ diameter. (c) 10λ diameter.

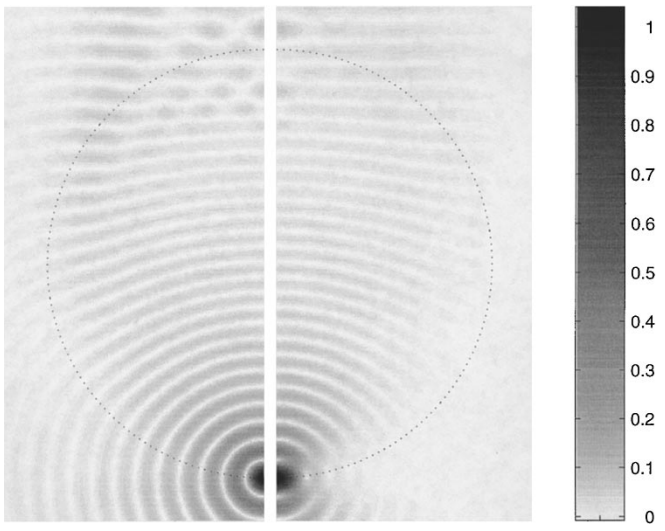

Fig. 9. Snapshot of the electric field near a 10λ-diameter spherical Luneburg lens excited by a Hertzian dipole. (a) H-plane. (b) E-plane.

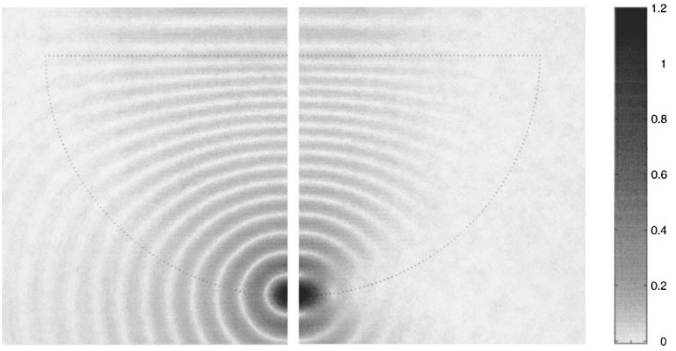

Fig. 11. Snapshot of the electric field near a 10λ-diameter half Maxwell fish eye excited by a Hertzian dipole.

cannot steer the radiating beam by moving the antenna feed. Second, there is some reflection when the wave leaves the lens because of the abrupt change in permittivity, resulting in lower efficiency. The field distribution in a half Maxwell fish eye is shown in Fig. 11.

V. Conclusion

The FEM using mixed edge-nodal basis functions and cylindrical PML is an efficient and accurate method for the analysis of radiation problems. The use of edge elements to expand the transverse field components avoids the problem of spurious modes in the FEM formulation. The use of cylindrical PML for mesh truncation allows an efficient computational domain for almost any problem geometry and it can be made very accurate, allowing the PML to be placed near the problem geometry. Numerical examples show that the method is accurate and highly efficient and it is capable of handling realistic sized radiating systems.

References

[1] D. E. Baker, "Pattern prediction of broadband monopole antennas on finite groundplanes using the BOR moment method," *Microwave J.*, vol. 31, pp. 153–164, 1988.

[2] A. Berthon and R. P. Bills, "Integral equation analysis of radiating structures of revolution," *IEEE Trans. Antennas Propagat.*, vol. 37, pp. 159–170, Feb. 1989.

[3] P. Steyn and D. B. Davidson, "A moment method formulation for electromagnetic radiation and scattering from composite bodies of revolution," in *9th Annu. Rev. Progress Appl. Computat. Electromagn.*, Monterey, CA, Mar. 1993, vol. I, pp. 64–71.

[4] J. Liu, J. Wang, and Y. Gao, "Computation of E-field distribution of low gain antenna on conducting body of revolution," in *11th Annu. Rev. Progress Appl. Computat. Electromagn.*, Monterey, CA, Mar. 1995, vol. II, pp. 687–694.

[5] F. L. Teixeira and J. R. Bergman, "B-spline basis functions for moment-method analysis of axisymmetric reflector antennas," *Microwave Opt. Tech. Lett.*, vol. 14, pp. 188–191, 1997.

[6] K. K. Mei, "Unimoment method for solving antenna and scattering problems," *IEEE Trans. Antennas Propagat.*, vol. AP-22, pp. 760–766, Nov. 1974.

[7] R. K. Gordon and R. Mittra, "Finite element analysis of axisymmetric radomes," *IEEE Trans. Antennas Propagat.*, vol. 41, pp. 975–981, July 1993.

[8] G. C. Chinn, L. W. Epp, and D. J. Hoppe, "A hybrid finite-element method for axisymmetric waveguide feed horns," *IEEE Trans. Antennas Propagat.*, vol. 44, pp. 280–285, Mar. 1996.

[9] E. Richalot, M. F. Wong, V. Fouad-Hanna, and H. Baudrand, "Analysis of radiating axisymmetric structures using a 2-D finite element and spherical mode expansion," *Microwave Opt. Tech. Lett.*, vol. 20, pp. 8–13, 1999.

[10] M. A. Morgan, S. K. Chang, and K. K. Mei, "Coupled azimuth potentials for electromagnetic field problems in inhomogeneous axially symmetric media," *IEEE Trans. Antennas Propagat.*, vol. 25, pp. 413–417, May 1977.

[11] M. A. Morgan, C. H. Chen, S. C. Hill, and P. W. Barber, "Finite-element-boundary integral formulation for electromagnetic scattering," *Wave Motion*, vol. 6, pp. 91–103, 1984.

[12] A. D. Greenwood and J. M. Jin, "Computation of the RCS of a complex BOR using FEM with coupled azimuth potentials and PML," *Electromagn.*, vol. 19, pp. 147–170, 1999.

[13] _____, "A novel, efficient algorithm for scattering from a complex BOR using mixed finite elements and cylindrical PML," *IEEE Trans. Antennas Propagat.*, vol. 47, pp. 620–629, Apr. 1999.

[14] J. F. Lee, G. M. Wilkins, and R. Mittra, "Finite-element analysis of an axisymmetric cavity resonator using a hybrid edge element technique," *IEEE Trans. Microwave Theory Tech.*, vol. 41, pp. 1981–1987, Nov. 1993.

[15] G. M. Wilkins, M. Swaminathan, and J. F. Lee, "Waveguide mode solution using a hybrid edge-element approach," *Int. J. Microwave Millimeter-Wave Comput. Aided Eng.*, vol. 2, pp. 122–130, 1995.

[16] G. C. Chinn, L. W. Epp, and G. M. Wilkins, "Determination of the eigenfrequencies of a ferrite-filled cylindrical cavity resonator using the finite element method," *IEEE Trans. Microwave Theory Tech.*, vol. 43, pp. 1207–1209, Nov. 1995.

[17] W. C. Chew, J. M. Jin, and E. Michielssen, "Complex coordinate stretching as a generalized absorbing boundary condition," *Microwave Opt. Tech. Lett.*, vol. 15, pp. 363–369, 1997.

[18] J. Maloney, M. Kesler, and G. Smith, "Generalization of PML to cylindrical geometries," in *13th Annu. Rev. Progress Appl. Computat. Electromagn.*, Monterey, CA, vol. II, pp. 900–908, Mar. 1997.

[19] F. L. Teixeira and W. C. Chew, "Systematic derivation of anisotropic PML absorbing media in cylindrical and spherical coordinates," *IEEE Microwave Guided Wave Lett.*, vol. 7, pp. 371–373, 1997.

[20] J. M. Jin, *The Finite Element Method in Electromagnetics*. New York: Wiley, 1993.

[21] M. F. Wong, M. Prak, and V. Fouad-Hanna, "Axisymmetric edge-based finite element formulation for bodies of revolution: Application to dielectric resonators," in *IEEE MTT-S Dig.*, May 1995, pp. 285–288.

[22] M. J. Al-Hakkak and Y. T. Lo, "Circular waveguides and horns with anisotropic and corrugated boundaries," Tech. Rep. 73-3, Antenna Lab., Dept. Elect. Eng., Univ. Illinois, Urbana, IL, 1973.

[23] R. K. Luneburg, *The Mathematical Theory of Optics*. Providence, RI: Brown Univ. Press, 1944.

[24] P. Rozenfeld, "The electromagnetic theory of three-dimensional inhomogeneous lenses," *IEEE Trans. Antennas Propagat.*, vol. AP-24, pp. 365–370, May 1976.

[25] J. C. Maxwell, *Scientific Papers—I*. New York: Dover, 1860.

Andrew D. Greenwood (S'90–M'98), for a photograph and biography, see p. 629 of the April 1999 issue of this Transactions.

Jian-Ming Jin (S'87–M'89–SM'94), for a photograph and biography, see p. 629 of the April 1999 issue of this Transactions.